

Model Predictive Trajectory Planning for Human-Robot Handovers

Thies Oelerich¹, Christian Hartl-Nesic¹, and Andreas Kugi^{1,2}

¹Automation and Control Institute (ACIN), TU Wien, Vienna, Austria

²AIT Austrian Institute of Technology GmbH, Vienna, Austria

Published at [1]

Abstract

This work develops a novel trajectory planner for human-robot handovers. The handover requirements can naturally be handled by a path-following-based model predictive controller, where the path progress serves as a progress measure of the handover. Moreover, the deviations from the path are used to follow human motion by adapting the path deviation bounds with a handover location prediction. A Gaussian process regression model, which is trained on known handover trajectories, is employed for this prediction. Experiments with a collaborative 7-DoF robotic manipulator show the effectiveness and versatility of the proposed approach.

1 Introduction

As robots become more capable at a high pace, they are expected to solve increasingly complex problems. Dynamically changing environments are challenging for robots to navigate and act in. A demanding and vital field in this context is human-robot interaction. As human intentions are hard to model, robots need to be able to quickly and reliably react to human motions while respecting dynamic and kinematic constraints. Human-robot handovers are a basic yet complex case of human-robot interactions.

This work uses a novel path-following-based trajectory planner for a robotic manipulator to realize natural human-robot handovers. A motion planning problem is solved online to enable the robot to react to the human behavior and the predictions of the human behavior.

Motion planning in robotics is a well-studied problem where many solution methods exist. Popular solutions are based on optimization [2, 3], sampling [4–6], or learning [7, 8]. This work focuses on optimization-based planning, precisely model predictive control (MPC), which is a popular optimization-based framework to plan motions and respect constraints [2, 9, 10]. It uses a receding time horizon to plan locally optimal trajectories based on a cost function at each time step. Path-following control is the first choice when a task is specified as a geometric path to be followed, as in [11, 12]. Such a formulation allows explicit control over the time evolution of the robot’s motion, such as controlling deviations from the path based on specific directions, as done in [13]. This paper proposes a path-following formulation to implement handover requirements naturally. Human-robot handovers can be interpreted as a path-following problem with a continuously changing and uncertain path. As the latter complicates the path-following task, existing solutions using MPC for handovers consider the handover point as the final goal but do not have a reference path. In [10], a grasping configuration is first computed, which is then reached by a suitable cost function in the MPC. A similar cost function is also used in [14] with a desired reach time. A more advanced

objective, utilizing a tracking cost, ergonomics, safety, and visibility, is employed in [15]. This work also applies a constant-velocity model to predict the human motion.

Motion planning in a human-robot handover scenario significantly benefits from predictions of the human motions. Thus, the path-following MPC formulation used in this work must react online to the human movements. Model predictive controller systematically incorporate such a behavior. A model for human motion is considered in addition to a model of the handover location. The handover location consists of a position and an orientation, which is the desired final pose of the robot's end-effector. It is unknown prior to the handover and may change during the handover. Previous works commonly use Gaussian process regression (GPR) to model unknown dynamics, as in [16, 17], which provides a predictive distribution instead of a most likely next state. GPR is used in [18, 19] for human-robot interaction to predict human motions during the interaction. Utilizing dynamic movement primitives, [20] manages to predict human handover trajectories. Several deep-learning methods for motion predictions are reviewed in [21].

In this work, a path-following-based MPC is combined with a GPR model to predict the handover location and its uncertainty measure. The path-following formulation is exploited to achieve successful handovers. The decomposition of the motion in the path direction and orthogonal to it allows us to interpret the motion along the path as the progress of the handover task and to use the directions orthogonal to the path for online adaptations and to synchronize the motion between the human and the robot.

The main contributions of this paper are as follows:

- the application of path-following MPC to human-robot handovers where the robot can move forward and backwards along the path based on the human motion,
- systematically taking into account the uncertainty of the handover location, and
- the adaption of the path error bounds during the handover to guide the robot towards the handover point and keep the human safe.

2 Successful Handovers

Human-robot handovers are complex interactions where the two actors, robot and human, have to be able to react to each other and move in a partially predictable way. The most essential requirements for a successful handover, inspired by [10, 22, 23], are:

- *Convergence*: The handover motions of both actors end at a common pose called the handover location.
- *Synchronization*: The time for the handover location is synchronized such that both actors reach it simultaneously.
- *Predictability*: The movements of each actor is predictable to let the other actor infer their intentions.
- *Safety*: Any collisions between the two actors are avoided.

A path-following-based formulation naturally fulfills these requirements. This formulation is further detailed in Section 4 based on the controller outlined in Section 3.

3 BoundMPC

In this section, a short overview of the path-following MPC is given. The formulation used in this work is inspired by a framework developed by the authors in a previous work called BoundMPC [24]. A schematic is shown in Fig. 1. In this formulation, the desired robot motion is given by position and orientation reference paths $\pi_p(\phi)$ and $\pi_o(\phi)$ with the path parameter ϕ , which must be followed by the robot's end-effector with position $\mathbf{p}_r(t)$ and rotation matrix $\mathbf{R}_r(t)$ in Cartesian space. Bounds limit the deviation of the planned trajectory from the reference path. Thus, the formulation makes the robot's end-effector move through a bounded volume in Cartesian space. As a special case, piecewise linear reference paths are used to connect the via-points.

The core of the formulation is based on a decomposition of the position path error $\mathbf{e}_{p,r} = \mathbf{p}_r(t) - \pi_p(\phi)$ and orientation path error $\mathbf{e}_{o,r}$ into tangential and orthogonal directions. The position path error $\mathbf{e}_{p,r}$ is decomposed into the direction π_p' tangential to the path and the two basic directions $\mathbf{b}_{p,1}$ and $\mathbf{b}_{p,2}$ orthogonal to the path, where $(\cdot)'$ denotes the partial derivative w.r.t. the path parameter ϕ . This results in the representation

$$\mathbf{e}_{p,r,\phi}^T = \begin{bmatrix} e_{p,r,1}^\perp & e_{p,r,2}^\perp & e_{p,r}^\parallel \end{bmatrix} \quad (1)$$

in the path system. BoundMPC minimizes the tangential error $e_{p,r}^\parallel$ and bounds the orthogonal errors $e_{p,r,1}^\perp$ and $e_{p,r,2}^\perp$. Thus, the robot can exploit the orthogonal errors to optimize its end-effector trajectory while following the path. The orientation path error $\mathbf{e}_{o,r} = \text{Log}(\mathbf{R}_r(t)\text{Exp}(\pi_o(\phi))^T)$ is obtained using matrix exponential and logarithm functions, it is defined in the Lie space for orientations; see [25] for more details on this concept. Decomposition is performed using the direction \mathbf{b}_{ω_r} along the path and the basic directions $\mathbf{b}_{o,1}$ and $\mathbf{b}_{o,2}$ orthogonal to the path. Hence, the orientation error in the path system reads as

$$\mathbf{e}_{o,r,\phi}^T = \begin{bmatrix} e_{o,r,1}^\perp & e_{o,r,2}^\perp & e_{o,r}^\parallel \end{bmatrix}, \quad (2)$$

where the individual components $e_{o,r,2}^\perp$, $e_{o,r}^\parallel$, and $e_{o,r,1}^\perp$ are

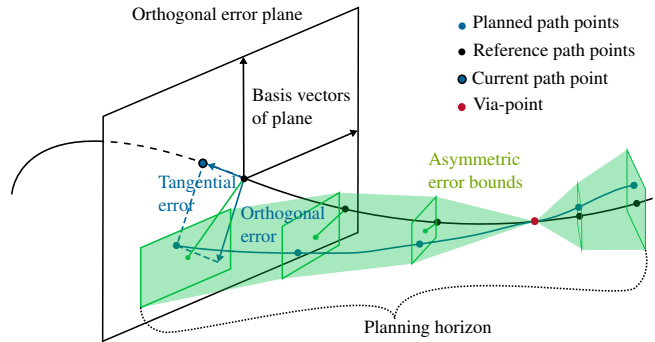


Figure 1: Schematic working principle of BoundMPC [24].

the roll, pitch, and yaw angles, respectively, in the coordinate system defined by the orientation direction vectors.

For more information, the reader is referred to [24]

4 Extensions for Human-Robot Handovers

The previous work [24] is extended by adapting the MPC such that a handover between a human and a robotic manipulator is possible according to the requirements formulated in Section 2. The prediction of the handover location is detailed in Section 4.3, and convergence of the robot's motion is ensured by adapting the error bounds described in Section 4.5 and adding a terminal cost described in Section 4.6 (*Convergence*). The error bounds constrain the robot's motion, allowing only limited motion orthogonal to the path (*Predictability*). Furthermore, combining the desired path state with error bounds avoids collisions between humans and robots, as discussed in Section 4.5 (*Safety*). Lastly, the path progress synchronizes the humans and robots motions as described in Section 4.4 (*Synchronization*).

The handover scenario is depicted in Fig. 2 with the predicted handover location distribution $\mathbf{p}_{HO} \sim \mathcal{N}(\mu_{HO}, \Sigma_{HO})$ and the current position of the human hand \mathbf{p}_h and the robot's end-effector \mathbf{p}_r . The adapted handover location used by the MPC $\tilde{\mathbf{p}}_{HO}$ is given by an interpolation between μ_{HO} and \mathbf{p}_h . As the human hand approaches the handover location, a prediction is no longer needed, and thus $\tilde{\mathbf{p}}_{HO} \rightarrow \mathbf{p}_h$. On the contrary, when \mathbf{p}_h is far from \mathbf{p}_{HO} , the handover location can only be inferred from the prediction model, meaning $\tilde{\mathbf{p}}_{HO} \rightarrow \mu_{HO}$. This is further detailed in Section 4.3.3.

4.1 Optimal control problem

In this section, the optimal control problem from the previous work [24] is adapted for human-robot handovers, which

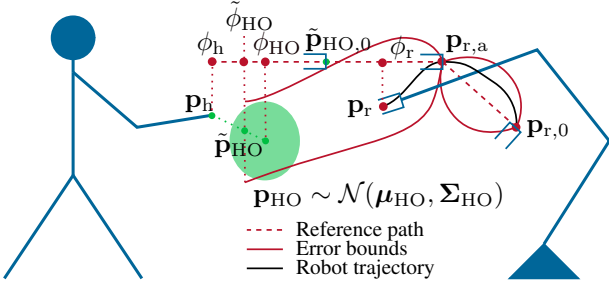


Figure 2: Visualization of the considered human-robot handover situation. The predicted handover location distribution \mathbf{p}_{HO} which determines the error bounds is visualized by the green circle. As the human is already close the handover location, the adapted handover location $\tilde{\mathbf{p}}_{\text{HO}}$ is a linear interpolation between the current human position \mathbf{p}_{h} and the predicted position $\boldsymbol{\mu}_{\text{HO}}$. The reference orientations at $\tilde{\mathbf{p}}_{\text{HO},0}$, $\mathbf{p}_{\text{r},a}$ and $\mathbf{p}_{\text{r},0}$ are indicated by a gripper symbol.

reads as

$$\min_{\substack{\mathbf{u}_1, \dots, \mathbf{u}_N, \\ \mathbf{x}_1, \dots, \mathbf{x}_N, \\ \boldsymbol{\xi}_1, \dots, \boldsymbol{\xi}_N, \\ v_1, \dots, v_N}} J_{\text{T}}(\mathbf{x}_N, \boldsymbol{\xi}_N, \mathbf{u}_N, v_N) + \sum_{i=1}^N l(\mathbf{x}_i, \boldsymbol{\xi}_i, \mathbf{u}_i, v_i) \quad (3a)$$

$$\text{s.t. } \mathbf{x}_{i+1} = \Phi \mathbf{x}_i + \Gamma_0 \mathbf{u}_i + \Gamma_1 \mathbf{u}_{i+1}, \quad i = 0, \dots, N-1 \quad (3b)$$

$$\boldsymbol{\xi}_{i+1} = \Phi_{\boldsymbol{\xi}} \boldsymbol{\xi}_i + \Gamma_{0,\boldsymbol{\xi}} v_i + \Gamma_{1,\boldsymbol{\xi}} v_{i+1}, \quad i = 0, \dots, N-1 \quad (3c)$$

$$\mathbf{x}_0 = \mathbf{x}_{\text{init}} \quad (3d)$$

$$\mathbf{u}_0 = \mathbf{u}_{\text{init}} \quad (3e)$$

$$\boldsymbol{\xi}_0 = \boldsymbol{\xi}_{\text{init}} \quad (3f)$$

$$v_0 = v_{\text{init}} \quad (3g)$$

$$\underline{\mathbf{x}} \leq \mathbf{x}_{i+1} \leq \bar{\mathbf{x}} \quad (3h)$$

$$\underline{\mathbf{u}} \leq \mathbf{u}_{i+1} \leq \bar{\mathbf{u}} \quad (3i)$$

$$\dot{\phi}_{\text{d}} = \dot{\phi}_{\text{d,max}} \tanh(s(d_{\text{r,HO}} - d_{\text{h,HO}} + b)) \quad (3j)$$

$$\Psi_{\text{p},m,\text{lower}}(\phi_i) \leq e_{\text{p},r,m}^{\perp} \leq \Psi_{\text{p},m,\text{upper}}(\phi_i), \quad m = 1, 2 \quad (3k)$$

$$\Psi_{\text{o},m,\text{lower}}(\phi_i) \leq e_{\text{o},r,m}^{\perp} \leq \Psi_{\text{o},m,\text{upper}}(\phi_i), \quad m = 1, 2. \quad (3l)$$

The robot joint and path dynamics are the discrete-time linear systems (3b) and (3c), respectively. The states and inputs for these systems have the initial conditions (3d)-(3g) and bounds (3h) and (3i).

The extensions to the previous work are the motion synchronization (3j) explained in Section 4.4, the bounds (3k) and (3l) explained in Section 4.5, and the removal of the constraint $\dot{\phi}_{i+1} \geq 0$, which allows the robot to move backwards along the path, i.e., $\dot{\phi}_{i+1} \leq 0$ is permitted. Furthermore, the cost function (3a) is extended by the terminal cost $J_{\text{T}}(\mathbf{x}_N, \boldsymbol{\xi}_N, \mathbf{u}_N, v_N)$. The stage cost $l(\mathbf{x}_i, \boldsymbol{\xi}_i, \mathbf{u}_i, v_i)$ is still used to minimize the tangential path error and reach the desired path state $\boldsymbol{\xi}_{\text{d}}$. For more information, see [24].

4.2 Reference paths

The reference paths for the robot's end-effector $\pi_{\text{p}}(\phi)$ and $\pi_{\text{o}}(\phi)$ are determined at the beginning of the handover and are kept constant during the handover. This is based on the

assumption that the handover location distribution is sufficiently accurate and that the actual handover location will not deviate significantly. The robot is assumed to start at a specific position $\mathbf{p}_{\text{r},0}$ from which it will move through an approach position $\mathbf{p}_{\text{r},a}$ towards the handover location $\tilde{\mathbf{p}}_{\text{HO}}$, see Fig. 2. The linear path from $\mathbf{p}_{\text{r},0}$ to the initially estimated handover location $\tilde{\mathbf{p}}_{\text{HO},0}$ is used as the reference path $\pi_{\text{p}}(\phi)$. The actual handover location will generally deviate from the path, which is accounted for by adapting the error bounds in Section 4.5 and the terminal costs in Section 4.6. This approach allows the use of the path parameter ϕ as the progress of the handover. Thus, the path velocity $\dot{\phi}$ serves to synchronize the robot and human motion. The orientation reference path $\pi_{\text{o}}(\phi)$ is also determined from the initially estimated handover location $\tilde{\mathbf{p}}_{\text{HO},0}$. The reference path $\pi_{\text{o}}(\phi)$ is chosen such that the gripper is oriented towards the human hand at $\tilde{\mathbf{p}}_{\text{HO},0}$, as indicated by the gripper symbols in Fig. 2.

4.3 Handover Location Prediction

As stated in Section 2, both actors must move to a mutual handover location (*Convergence*). However, this location is unknown to the robot, and thus, a prediction model is needed to estimate it. In this section, a Gaussian process model is proposed to predict the handover location \mathbf{p}_{HO} in Section 4.3.1. As the human hand approaches the actual handover location, this prediction gradually switches towards the actual position of the human hand \mathbf{p}_{h} , as detailed in Section 4.3.3.

4.3.1 Gaussian Process Model

The purpose of this model is to predict the distribution of the position of the Cartesian handover location $\mathbf{p}_{\text{HO}} \in \mathbb{R}^3$ from the measured current hand position \mathbf{p}_{h} . This work uses a Gaussian process regression model for this task. Thus, the distribution of \mathbf{p}_{HO} is given by the Gaussian distribution

$$\mathbf{p}_{\text{HO}} \sim \mathcal{N}(\boldsymbol{\mu}_{\text{HO}}, \boldsymbol{\Sigma}_{\text{HO}}), \quad (4)$$

with mean $\boldsymbol{\mu}_{\text{HO}}$ and covariance matrix $\boldsymbol{\Sigma}_{\text{HO}}$. By assuming that the components of \mathbf{p}_{HO} are independent, it is possible to train separate prediction models for each spatial component. The training data for each of the three models $j \in [x, y, z]$ consists of N known handover trajectories with n_k data points in the k -th trajectory resulting in a total of $n = \sum_{k=1}^N n_k$ data points. All data points are summarized in the input matrix $\mathbf{X}_{\text{train}} \in \mathbb{R}^{n \times 6}$ and the output vector $\mathbf{y}_{\text{train}} \in \mathbb{R}^n$, where each row is given by

$$(\mathbf{x}_{\text{train},i}^{\text{T}}, y_{\text{train},i}) = \left(\begin{bmatrix} \mathbf{p}_{\text{h},\text{train},i} \\ \mathbf{v}_{\text{h},\text{train},i} \end{bmatrix}^{\text{T}}, p_{\text{HO},\text{train},j,i} \right), \quad (5)$$

with $\mathbf{x}_{\text{train},i}$ containing the human position $\mathbf{p}_{\text{h},\text{train},i} \in \mathbb{R}^3$ and velocity $\mathbf{v}_{\text{h},\text{train},i} \in \mathbb{R}^3$, $i = 1, \dots, n$ and the corresponding output handover location

$$\mathbf{p}_{\text{HO},\text{train},i}^{\text{T}} = [p_{\text{HO},\text{train},x,i}, p_{\text{HO},\text{train},y,i}, p_{\text{HO},\text{train},z,i}]. \quad (6)$$

Given a scalar kernel function $k(\mathbf{x}_{\text{train},i}, \mathbf{x}_{\text{train},j})$, the matrix $\mathbf{K}(\mathbf{X}_{\text{train}}, \mathbf{X}_{\text{train}}) \in \mathbb{R}^{n \times n}$ is the result of applying this kernel function to all pairs of training input points $\mathbf{x}_{\text{train},i}$

contained in $\mathbf{X}_{\text{train}}$. In this work, the squared exponential kernel function is used. A test input point \mathbf{x}_{test} then leads to the predicted output mean and covariance [26]

$$\mu_{\text{HO},j} = \mathbf{k}_{\text{test}}^T (\mathbf{K} + \sigma_n^2 \mathbf{I})^{-1} \mathbf{y}_{\text{train}} \quad (7a)$$

$$\Sigma_{\text{HO},j} = k(\mathbf{x}_{\text{test}}, \mathbf{x}_{\text{test}}) - \mathbf{k}_{\text{test}}^T (\mathbf{K} + \sigma_n^2 \mathbf{I})^{-1} \mathbf{k}_{\text{test}} \quad (7b)$$

with \mathbf{k}_{test} being the vector of kernel function values between the test point \mathbf{x}_{test} and all training points $\mathbf{x}_{\text{train},i}$, and σ_n^2 is the variance of the assumed zero mean measurement noise of $\mathbf{y}_{\text{train}}$. The covariance values $\Sigma_{\text{HO},j}$ determine the diagonal of Σ_{HO} . All other values of Σ_{HO} are zero due to the assumed independence. For more information on Gaussian process regression, the reader is referred to [26].

4.3.2 Projection of the Handover Prediction

The prediction of the handover location distribution \mathbf{p}_{HO} is done in the global coordinate system. In order to use it within the path-following MPC, the handover location distribution is projected onto the path π_p using the basis vectors $\mathbf{b}_{p,1}$ and $\mathbf{b}_{p,2}$ of the path segment in which the handover takes place. Its mean is represented as

$$\mu_{\text{HO},\phi}^T = [e_{p,\text{HO},1}^\perp \quad e_{p,\text{HO},2}^\perp \quad \phi_{\text{HO}}] \quad (8)$$

with

$$\phi_{\text{HO}} = \phi_0 + ((\mu_{\text{HO}} - \pi_p(\phi_0))^T \pi_p'(\phi_{\text{HO}})) \quad (9a)$$

$$\begin{bmatrix} e_{p,\text{HO},1}^\perp \\ e_{p,\text{HO},2}^\perp \end{bmatrix} = \begin{bmatrix} \mathbf{b}_{p,1}^T \\ \mathbf{b}_{p,2}^T \end{bmatrix} (\mu_{\text{HO}} - \pi(\phi_{\text{HO}})), \quad (9b)$$

where $e_{p,\text{HO},1}^\perp$ and $e_{p,\text{HO},2}^\perp$ are the orthogonal deviations from the path, ϕ_{HO} is the path parameter at which the handover location takes place, $\pi(\phi_{\text{HO}})$ is the point on the reference path closest to μ_{HO} , and ϕ_0 is the path parameter at $\mathbf{p}_{r,a}$.

In addition to the mean μ_{HO} , the prediction model from Section 4.3 also provides the uncertainty Σ_{HO} of the handover location in the global coordinate system. The basis vectors $\mathbf{b}_{p,1}$ and $\mathbf{b}_{p,2}$ are used to obtain

$$\Sigma_{\text{HO},\phi} = \begin{bmatrix} \mathbf{b}_{p,1}^T \\ \mathbf{b}_{p,2}^T \end{bmatrix} \Sigma_{\text{HO}} [\mathbf{b}_{p,1} \mathbf{b}_{p,2}] \quad (10)$$

as the uncertainty of the handover location distribution \mathbf{p}_{HO} in the orthogonal directions. The projected matrix $\Sigma_{\text{HO},\phi}$ represents an ellipse with half axis r_1 and r_2 and angle θ from the positive horizontal axis to r_1 , while the bounding of the orthogonal errors $e_{p,\text{HO},1}^\perp$ and $e_{p,\text{HO},2}^\perp$ is performed by box constraints. Thus, it is necessary to find the smallest axis-aligned rectangle that includes the ellipse given by r_1 , r_2 , and θ in the coordinates with the basis vectors $\mathbf{b}_{p,1}$ and $\mathbf{b}_{p,2}$. This rectangle is given by the maximum coordinates in the basis direction $\mathbf{b}_{p,1}$ and $\mathbf{b}_{p,2}$, called $x_{1,\text{max}}$ and $x_{2,\text{max}}$, respectively. Thus, the approximation of the handover location distribution \mathbf{p}_{HO} in the path coordinates is defined by the box constraints $(e_{p,\text{HO},1}^\perp - x_{1,\text{max}}, e_{p,\text{HO},1}^\perp + x_{1,\text{max}})$ for the basis direction $\mathbf{b}_{p,1}$ and $(e_{p,\text{HO},2}^\perp - x_{2,\text{max}}, e_{p,\text{HO},2}^\perp + x_{2,\text{max}})$ for the basis direction $\mathbf{b}_{p,2}$ at the path parameter $\phi = \phi_{\text{HO}}$. Note that the uncertainty in the path parameter ϕ_{HO} is not considered.

4.3.3 Prediction Model Adaptions

The handover location becomes more confident as the robot converges towards the human hand. Eventually, the prediction model (7) will not be needed anymore, and the measured human position \mathbf{p}_h is used instead. The vector $\mathbf{p}_{h,\phi}^T = [e_{p,h,1}^\perp, e_{p,h,2}^\perp, \phi_h]$ represents the current human position \mathbf{p}_h in the path system similar to (8) and (9).

The estimated handover location is given as the linear interpolation

$$\begin{aligned} \tilde{\mathbf{p}}_{\text{HO},\phi}^T &= [\tilde{e}_{p,\text{HO},1}^\perp \quad \tilde{e}_{p,\text{HO},2}^\perp \quad \tilde{\phi}_{\text{HO}}] \\ &= w_{\text{pred}}(\alpha_p, d_p) \mu_{\text{HO},\phi}^T + (1 - w_{\text{pred}}(\alpha_p, d_p)) \mathbf{p}_{h,\phi}^T \end{aligned} \quad (11)$$

between $\mathbf{p}_{h,\phi}$ and $\mu_{\text{HO},\phi}$ using the weight $0 \leq w_{\text{pred}} \leq 1$ with

$$w_{\text{pred}}(\alpha_p, d_p) = \frac{1}{2} + \frac{1}{2} \tanh(\alpha_p d_{\text{pred}} - d_p) \quad (12)$$

and $d_{\text{pred}} = \phi_h - \phi_{\text{HO}}$ as the distance of the human hand from the handover location in path direction. The parameters α_p and d_p of the function (12) control the distances at which the interpolation starts and stops.

Furthermore, as the human hand approaches the handover location, i.e., $d_{\text{pred}} \rightarrow 0$, the uncertainty of the handover location becomes smaller. Thus, the projected uncertainty values $x_{1,\text{max}}$ and $x_{2,\text{max}}$ are set to zero for $w_{\text{pred}} \approx 1$. A linear interpolation, as in (11), is not necessary in this case, as it is assumed that the uncertainty of the model already decreases when $d_{\text{pred}} \rightarrow 0$.

4.3.4 Orientation Prediction

The orientation of the handover location is not part of the Gaussian process model; instead, the current rotation matrix of the human hand \mathbf{R}_h is used. Again, \mathbf{R}_h is given in the global coordinate system and needs to be projected onto the path. Our previous work [24] shows that projecting \mathbf{R}_h onto the path is equivalent to computing the RPY angles in the coordinate system given by the orientation basis vectors $\mathbf{b}_{o,1}$, $\mathbf{b}_{o,2}$, and the normed angular velocity vector \mathbf{b}_{ω_r} of the last reference path segment. Using the projection matrix

$$\mathbf{R}_{\text{proj}} = [\mathbf{b}_{o,2} \mid \mathbf{b}_{\omega_r} \mid \mathbf{b}_{o,1}], \quad (13)$$

the rotation matrix \mathbf{R}_h is projected according to

$$\mathbf{R}_{\text{RPY}} = \mathbf{R}_{\text{proj}}^T \mathbf{R}_h \mathbf{R}_{\text{proj}} \quad (14)$$

into the coordinate system defined by \mathbf{R}_{proj} , from which the RPY angles are calculated. Thus, the yaw, roll, and pitch angles of \mathbf{R}_{RPY} are the orthogonal orientation errors $e_{o,h,1}^\perp$ and $e_{o,h,2}^\perp$ and the tangential orientation error $e_{o,h}^\parallel$ of \mathbf{R}_h , respectively.

Using this projection, the orientation goal w.r.t. the orientation path is given by $e_{o,h,1}^\perp$ and $e_{o,h,2}^\perp$. These orthogonal orientation errors are adapted according to

$$\tilde{e}_{o,h,i}^\perp = (1 - w_{\text{pred}}(\alpha_o, d_o)) e_{o,h,i}^\perp, \quad i = 1, 2, \quad (15)$$

with the parameters α_o and d_o , chosen similar to α_p and d_p , controlling the convergence of $\tilde{e}_{o,h,i}^\perp$ towards $e_{o,h,i}^\perp$ as

$d_{\text{pred}} \rightarrow 0$. Thus, the desired orientation errors $\tilde{e}_{o,h,i}^\perp$ are approximately 0 when the robot is close to the approach point $\mathbf{p}_{r,a}$ and arrives at the projected orientation of the human hand $e_{o,h,i}^\perp$ at the handover location. The handover location $\tilde{\mathbf{p}}_{\text{HO}}$ is assumed to be close to $\tilde{\mathbf{p}}_{\text{HO},0}$ such that minimizing $e_{o,h}^\perp$ leads to the desired approach orientation for $\tilde{\mathbf{p}}_{\text{HO}}$.

4.4 Motion Synchronization

The BoundMPC formulation includes a desired path state $\xi_{\text{d}}^T = [\phi_{\text{d}}, \dot{\phi}_{\text{d}}, \ddot{\phi}_{\text{d}}]$ in its objective function (3a), which is used to control the path progress [24]. In this work, ξ_{d} enables the motion synchronization between the human and the robot as required for a handover. Specifically, ϕ_{d} is combined with the error bounds in Section 4.5 to reach the handover location (*Convergence*), while $\dot{\phi}_{\text{d}}$ is used to synchronize the human and the robot motion speed (*Synchronization*). Setting

$$\phi_{\text{d}} = \tilde{\phi}_{\text{HO}} \quad (16)$$

ensures that the robot moves as far along the path as is necessary to reach the handover location.

Synchronizing the path progress of the human and the robot brings along that the handover location is reached approximately simultaneously by both actors. The signed distances of the path parameter of the current human hand position ϕ_{h} and the current robot position ϕ_{c} to the handover point $\tilde{\phi}_{\text{HO}}$ are

$$d_{\text{h,HO}}(t) = \phi_{\text{h}}(t) - \tilde{\phi}_{\text{HO}} \quad (17)$$

and

$$d_{\text{r,HO}}(t) = \tilde{\phi}_{\text{HO}} - \phi_{\text{c}}(t), \quad (18)$$

respectively. The desired speed along the path is chosen as

$$\dot{\phi}_{\text{d}} = \dot{\phi}_{\text{d,max}} \tanh(s(d_{\text{r,HO}} - d_{\text{h,HO}} + b)), \quad (19)$$

with the maximum speed $\dot{\phi}_{\text{d,max}}$ and the parameters s and b influencing the shape of the smooth function (19). Note that (19) can be interpreted as a P controller with saturation. The desired path velocity $\dot{\phi}_{\text{d}}$ in (19) can become negative if the human hand is further away from the handover location than the robot by an offset b , incentivizing the robot to slow down or move backwards along the path. In classical path-following control, the path velocity must be typically positive. This requirement is relaxed here to realize a more natural human-robot interaction.

4.5 Error Bounds

A successful handover requires the robot's end-effector position \mathbf{p}_{r} to converge to the position of the human hand \mathbf{p}_{h} at the handover point $\tilde{\mathbf{p}}_{\text{HO}}$ (*Convergence*). Furthermore, it is required that the robot moves predictably such that the human can anticipate the handover trajectory and does not collide with the human hand (*Predictability, Safety*).

The allowed deviations in orthogonal direction are determined by the error bounding functions in the position $\Psi_{\text{p},i,j}(\phi)$ and the orientation $\Psi_{\text{o},i,j}(\phi)$ for the basis directions $i = 1, 2$ and $j \in \{\text{upper}, \text{lower}\}$. Thus, there are a total of eight error bounding functions, i.e., one upper bound

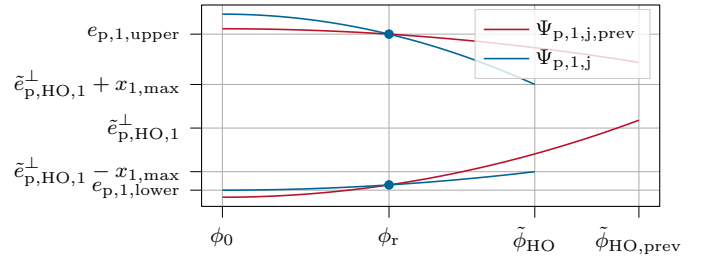


Figure 3: Error bounding functions for $e_{\text{p},\text{r},1}^\perp$ in two consecutive time steps where $\Psi_{\text{p},1,j,\text{prev}}$ and $\Psi_{\text{p},1,j}$ are the error functions in the first and second time step, respectively. The bounding functions range from the start of the handover segment at ϕ_0 to the handover location at $\tilde{\phi}_{\text{HO}}$. The previous estimation of the handover location path parameter is $\tilde{\phi}_{\text{HO,prev}}$

($j = \text{upper}$) and one lower bound ($j = \text{lower}$) for each orthogonal direction in the position and orientation, which are updated in each time step.

Second-order functions serve as bounding functions. The replanning of the bounds is based on the bounds from the previous time step $\Psi_{\text{p},i,j,\text{prev}}$. A visual explanation of the adaptation for one orthogonal direction is given in Fig. 3. Specifically, the bounds at the new time step coincide with the bounds of the previous time step at the current path parameter ϕ_{r} with the values $\Psi_{\text{p},i,j}(\phi_{\text{r}}) = \Psi_{\text{p},i,j,\text{prev}}(\phi_{\text{r}}) = e_{\text{p},i,j}$. The other directions are adapted analogously.

The described adaption of the allowed orthogonal deviation from the reference paths ensures that, as the robot traverses the path, the bounds converge to the desired handover location (*Convergence*). As the bounds gradually narrow, the movement of the robot's end-effector becomes more restricted, ensuring that no sudden movements occur and the motion stays predictable (*Predictability*). Furthermore, the desired path parameter $\phi_{\text{d}} = \tilde{\phi}_{\text{HO}}$ from (16), in combination with the error bounds, ensures that the robot's end-effector does not collide with the human hand as the end-effector is incentivized to stay in front of the human hand (*Safety*).

4.6 Terminal Cost

With the specified error bounds from Section 4.5, the robot is incentivized to move to the goal. In order to further improve the goal-seeking behavior, a terminal cost term is added to the MPC formulation (3) (*Convergence*). A reasonable choice is the tracking cost

$$J_{\text{T}} = w_{\text{T,p}} \left\| \begin{bmatrix} e_{\text{p},\text{r},1}^\perp - \tilde{e}_{\text{p,HO},1}^\perp \\ e_{\text{p},\text{r},2}^\perp - \tilde{e}_{\text{p,HO},2}^\perp \end{bmatrix} \right\|_2^2 + w_{\text{T,o}} \left\| \begin{bmatrix} e_{\text{o},\text{r},1}^\perp - \tilde{e}_{\text{o,h},1}^\perp \\ e_{\text{o},\text{r},2}^\perp - \tilde{e}_{\text{o,h},2}^\perp \end{bmatrix} \right\|_2^2 \quad (20)$$

with the positive weights $w_{\text{T,p}}$ and $w_{\text{T,o}}$. Extending the cost (3a) by (20) makes the robot's end-effector converge to the adapted handover location $\tilde{\mathbf{p}}_{\text{HO}}$.

5 Handover Experiment

The performance of the developed MPC formulation is demonstrated by a human-to-robot handover experiment where a human hands a cup to the robot. The trajectories of the human hand and the robot's end effector are shown in

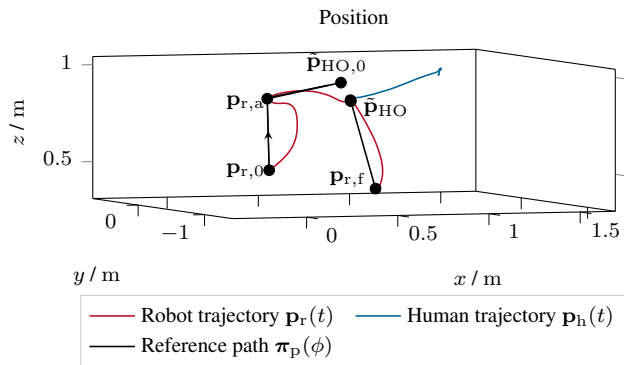


Figure 4: Position trajectories of the robot's end-effector $\mathbf{p}_r(t)$ and human hand $\mathbf{p}_h(t)$.

Fig. 4. The robot moves from an initial pose $\mathbf{p}_{r,0}$ to an approach point $\mathbf{p}_{r,a}$ from which it continues to perform the handover at $\tilde{\mathbf{p}}_{HO}$. The reference path is initially planned towards the first prediction of the handover location $\tilde{\mathbf{p}}_{HO,0}$. However, the robot deviates from this path to reach the actual handover location $\tilde{\mathbf{p}}_{HO}$, computed during the handover. Afterwards, a new reference path segment is planned from $\tilde{\mathbf{p}}_{HO}$ to the final pose $\mathbf{p}_{r,f}$ at which the robot puts the object down. Using OptiTrack, The cup is tracked instead of the human hand since it represents the object of interest. A video of the experiments is available at www.acin.tuwien.ac.at/42d1/.

Figure 5 shows the path parameter of the robot ϕ_r , the human ϕ_h , and the predicted handover location $\tilde{\phi}_{HO}$. The robot tries to synchronize this motion, which results in an approximately simultaneous arrival at the handover location $\tilde{\mathbf{p}}_{HO}$. However, the robot arrives slightly later due to the bound in the joint velocity \dot{q}_2 of axis 2, which limits the robot's end-effector velocity. This also shows that the kinematic limits are exploited but not violated. Furthermore, the robot slows down during $2\text{ s} < t < 2.5\text{ s}$ since the human has not started moving yet. For $t > 3\text{ s}$, the handover path location approaches $\tilde{\phi}_{HO} \approx \phi_h$ due to the adaption in (11).

Further insights can be gained from the orthogonal position errors $e_{p,r,1}^\perp$ and $e_{p,h,1}^\perp$ and orientation errors $e_{o,r,1}^\perp$ and $e_{o,h,1}^\perp$ shown in **Fig. 6**. The robot successfully traverses the via-point and enters the segment of the handover where the bounds are adapted to converge to the position of the human hand. The bounds are initially high due to the uncertainty of \mathbf{p}_{HO} and then narrow as the robot approaches the human hand. Note that a low orientation error is present at the final handover pose $\tilde{\mathbf{p}}_{HO}$ due to the weights $w_{T,p} > w_{T,o}$. This low error still allows reliable human-to-robot handovers.

6 Conclusion

This work proposes a novel trajectory planner for human-robot handovers. The planner is based on a path-following model predictive control (MPC) formulation where specific requirements for successful handovers are naturally encoded. A handover location prediction is developed based on Gaussian process regression, which predicts the final pose of the handover. This pose is then approached by projecting it into the path system and using a terminal cost in combination with Cartesian error-bound adaptations. These adaptations are made in each step to ensure that the robot reacts appropri-

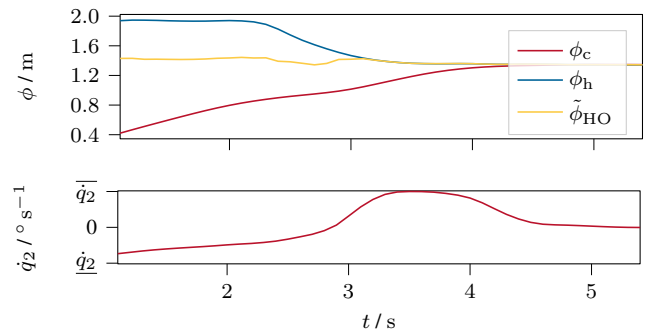


Figure 5: Path parameter of the robot, the human, and the predicted handover location. Additionally, the joint velocity \dot{q}_2 of axis 2 is shown with the velocity constraints $\underline{\dot{q}}_2$ and $\bar{\dot{q}}_2$.

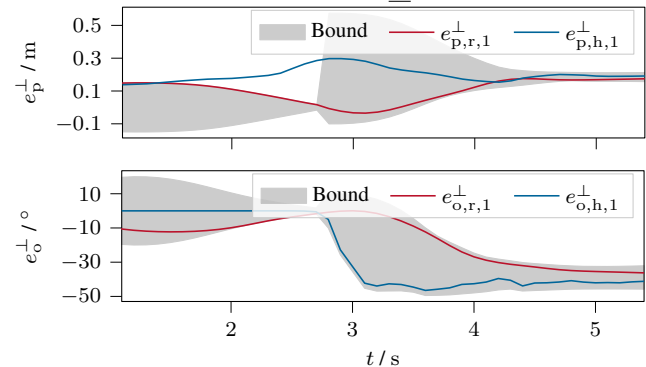


Figure 6: Orthogonal position errors $e_{p,r,1}^\perp$ and $e_{p,h,1}^\perp$ and orientation errors $e_{o,r,1}^\perp$ and $e_{o,h,1}^\perp$ during the handover. Only the part of the trajectory relevant to the handover is shown. The robot errors $e_{p,r,1}^\perp$ and $e_{o,r,1}^\perp$ remain within the bounds while the human errors $e_{p,h,1}^\perp$ and $e_{o,h,1}^\perp$ are unbounded.

ately to human motion. Finally, the feasibility of the proposed approach is demonstrated on a 7-DoF robotic manipulator, which receives an object from a human during a handover. Future work will deal with improvements to human motion prediction and applying the developed framework to other scenarios with dynamically changing environments and goals.

References

- [1] Thies Oelerich, Christian Hartl-Nesic, and Andreas Kugi. "Model Predictive Trajectory Planning for Human-Robot Handovers". In: *Proceedings of VDI Mechatroniktagung*. 2024, pp. 65–72. URL: https://www.vdi-mechatroniktagung.rwth-aachen.de/global/show_document.asp?id=aaaaaaaaacjcayqj&download=1 (visited on 04/05/2024).
- [2] Tobias Schoels et al. "CIAO*: MPC-based Safe Motion Planning in Predictable Dynamic Environments". In: *IFAC-PapersOnLine* 53.2 (2020), pp. 6555–6562. DOI: [10.1016/j.ifacol.2020.12.072](https://doi.org/10.1016/j.ifacol.2020.12.072).
- [3] John Schulman et al. "Motion Planning with Sequential Convex Optimization and Convex Collision Checking". In: *The International Journal of Robotics Research* 33.9 (2014), pp. 1251–1270. DOI: [10.1177/0278364914528132](https://doi.org/10.1177/0278364914528132).

- [4] Julius Jankowski et al. “VP-STO: Via-point-based Stochastic Trajectory Optimization for Reactive Robot Behavior”. In: *Proceedings of the IEEE International Conference on Robotics and Automation (ICRA)*. 2023, pp. 10125–10131. DOI: [10.1109/ICRA48891.2023.10160214](https://doi.org/10.1109/ICRA48891.2023.10160214).
- [5] Sven Mikael Persson and Inna Sharf. “Sampling-Based A* Algorithm for Robot Path-Planning”. In: *The International Journal of Robotics Research* 33.13 (2014), pp. 1683–1708. DOI: [10.1177/0278364914547786](https://doi.org/10.1177/0278364914547786).
- [6] Mohamed Elbanhawi and Milan Simic. “Sampling-Based Robot Motion Planning: A Review”. In: *IEEE Access* 2 (2014), pp. 56–77. DOI: [10.1109/ACCESS.2014.2302442](https://doi.org/10.1109/ACCESS.2014.2302442).
- [7] Takayuki Osa. “Motion Planning by Learning the Solution Manifold in Trajectory Optimization”. In: *The International Journal of Robotics Research* 41.3 (2022), pp. 281–311. DOI: [10.1177/02783649211044405](https://doi.org/10.1177/02783649211044405).
- [8] Joao Carvalho et al. “Motion Planning Diffusion: Learning and Planning of Robot Motions with Diffusion Models”. In: *Proceedings of the IEEE/RSJ International Conference on Intelligent Robots and Systems (IROS)*. 2023, pp. 1916–1923. DOI: [10.1109/IROS55552.2023.10342382](https://doi.org/10.1109/IROS55552.2023.10342382). (Visited on 12/20/2023).
- [9] M. Mahdi Ghazaei Ardakani et al. “Real-Time Trajectory Generation Using Model Predictive Control”. In: *Proceedings of the IEEE International Conference on Automation Science and Engineering (CASE)*. IEEE, 2015, pp. 942–948. DOI: [10.1109/CoASE.2015.7294220](https://doi.org/10.1109/CoASE.2015.7294220).
- [10] Wei Yang et al. “Model Predictive Control for Fluid Human-to-Robot Handovers”. In: *Proceedings of the International Conference on Robotics and Automation (ICRA)*. IEEE, 2022, pp. 6956–6962. DOI: [10.1109/ICRA46639.2022.9812109](https://doi.org/10.1109/ICRA46639.2022.9812109).
- [11] Alejandro Astudillo et al. “Varying-Radius Tunnel-Following NMPC for Robot Manipulators Using Sequential Convex Quadratic Programming”. In: *Proceedings of the Modeling, Estimation and Control Conference*. Vol. 55. 2022, pp. 345–352. DOI: [10.1016/j.ifacol.2022.11.208](https://doi.org/10.1016/j.ifacol.2022.11.208).
- [12] Niels Van Duijkeren et al. “Path-Following NMPC for Serial-Link Robot Manipulators Using a Path-Parametric System Reformulation”. In: *Proceedings of the European Control Conference (ECC)*. 2016, pp. 477–482. DOI: [10.1109/ECC.2016.7810330](https://doi.org/10.1109/ECC.2016.7810330).
- [13] Christian Hartl-Nesic, Tobias Glück, and Andreas Kugi. “Surface-Based Path Following Control: Application of Curved Tapes on 3-D Objects”. In: *IEEE Transactions on Robotics* 37.2 (2021), pp. 615–626. DOI: [10.1109/TRO.2020.3033721](https://doi.org/10.1109/TRO.2020.3033721).
- [14] Alap Kshirsagar et al. “Timing-Specified Controllers with Feedback for Human-Robot Handovers”. In: *Proceedings of the IEEE International Conference on Robot and Human Interactive Communication (RO-MAN)*. 2022, pp. 1313–1320. DOI: [10.1109/RO-MAN53752.2022.9900856](https://doi.org/10.1109/RO-MAN53752.2022.9900856).
- [15] Gianluca Corsini et al. “Nonlinear Model Predictive Control for Human-Robot Handover with Application to the Aerial Case”. In: *Proceedings of the IEEE/RSJ International Conference on Intelligent Robots and Systems (IROS)*. 2022, pp. 7597–7604. DOI: [10.1109/IROS47612.2022.9981045](https://doi.org/10.1109/IROS47612.2022.9981045).
- [16] Lukas Hewing, Juraj Kabzan, and Melanie N. Zeilinger. “Cautious Model Predictive Control Using Gaussian Process Regression”. In: *IEEE Transactions on Control Systems Technology* 28.6 (2020), pp. 2736–2743. DOI: [10.1109/TCST.2019.2949757](https://doi.org/10.1109/TCST.2019.2949757).
- [17] Johanna Bethge et al. “Model Predictive Control with Gaussian-Process-Supported Dynamical Constraints for Autonomous Vehicles”. In: *IFAC-PapersOnLine*. 22nd IFAC World Congress 56.2 (2023), pp. 507–512. DOI: [10.1016/j.ifacol.2023.10.1618](https://doi.org/10.1016/j.ifacol.2023.10.1618).
- [18] Shen Li et al. “Provably Safe and Efficient Motion Planning with Uncertain Human Dynamics”. In: *Proceedings of Robotics: Science and Systems*. 2021. DOI: [10.15607/rss.2021.xvii.050](https://doi.org/10.15607/rss.2021.xvii.050).
- [19] Min Wu et al. “On-Line Motion Prediction and Adaptive Control in Human-Robot Handover Tasks”. In: *Proceedings of the IEEE Workshop on Advanced Robotics and its Social Impacts, ARSO* (2019), pp. 1–6. DOI: [10.1109/ARSO46408.2019.8948750](https://doi.org/10.1109/ARSO46408.2019.8948750).
- [20] Dominik Widmann and Yiannis Karayiannidis. “Human Motion Prediction in Human-Robot Handovers Based on Dynamic Movement Primitives”. In: *Proceedings of the European Control Conference (ECC)*. 2018, pp. 2781–2787. DOI: [10.23919/ECC.2018.8550170](https://doi.org/10.23919/ECC.2018.8550170).
- [21] Kedi Lyu et al. “3D Human Motion Prediction: A Survey”. In: *Neurocomputing* 489 (2022), pp. 345–365. DOI: [10.1016/j.neucom.2022.02.045](https://doi.org/10.1016/j.neucom.2022.02.045).
- [22] Angeliki Zacharaki et al. “Safety Bounds in Human Robot Interaction: A Survey”. In: *Safety Science* 127 (2020), p. 104667. DOI: [10.1016/j.ssci.2020.104667](https://doi.org/10.1016/j.ssci.2020.104667).
- [23] Kyle Wayne Strabala et al. “Towards Seamless Human-Robot Handovers”. In: *Journal of Human-Robot Interaction* 2.1 (2013), pp. 112–132. DOI: [10.5898/jhri.2.1.strabala](https://doi.org/10.5898/jhri.2.1.strabala).
- [24] Thies Oelerich et al. *BoundMPC: Cartesian Trajectory Planning with Error Bounds Based on Model Predictive Control in the Joint Space*. 2024. arXiv: [2401.05057 \[cs\]](https://arxiv.org/abs/2401.05057).
- [25] Joan Solà, Jeremie Deray, and Dinesh Atchuthan. *A Micro Lie Theory for State Estimation in Robotics*. 2021. arXiv: [1812.01537 \[cs\]](https://arxiv.org/abs/1812.01537).

- [26] Carl Edward Rasmussen and Christopher K. I. Williams. *Gaussian Processes for Machine Learning*. Adaptive Computation and Machine Learning. Cambridge, Massachusetts: MIT Press, 2006.